QUASI-ELASTIC LIGHT SCATTERING BY DIFFUSIONAL FLUCTUATIONS IN RNASE SOLUTIONS

L. RIMAI, J. T. HICKMOTT, JR., T. COLE, *and* E. B. CAREW

From the Scientific Research Staff, Ford Motor Company, Dearborn, Michigan 48121. Dr. Carew's permanent address is The University of Michigan, Dearborn Campus.

ABSTRACT Using measurements of quasi-elastic light scattering spectra, we have investigated diffusional fluctuations of RNase. The diffusion coefficient for individual protein molecules, together with the corresponding calculated effective molecular radius R_{eff}, were determined. Between room temperature and the point of irreversible denaturation at 63.5°C, R_{eff} increased from 20–250 A. This is comparable to the plateau in R_{eff} of 300 A reached after about 200 min following chemical denaturation in 10 M urea. The measurements indicated the presence of a large size component even in the freshly prepared and chromatographically purified solutions. From the diffusion constants deduced for this large component we obtained effective sizes from 1000–5000 A. Concentration and temperature dependent measurements exclude the possibility that these large particles are impurities and indicate that they are the result of aggregations of RNase molecules.

INTRODUCTION

We have measured the diffusion constant of a relatively simple protein, RNase, by quasi-elastic light scattering, during both thermal and chemical denaturation. We have obtained the changes in effective molecular size during this transition. We have also shown the presence of a small concentration of aggregated material with particle size in the order of 3000 A to be present even in the fresh sample. These experiments make use of self-beating optical detection methods (1–3) to obtain the frequency shifts in the scattered light.

The concentration of the aggregate was small at room temperature but could be increased by heat and chemical denaturing agents. A short, nongel-inducing exposure to high temperature increased irreversibly this large particle concentration. The possibility that the aggregate might be a contaminant was eliminated by concentration dependence studies. There was an indication that the line width of the spectrum originating from the aggregated material had a nontranslational component. This component may represent a rate process related to the aggregate formation.

Experimentally the problem involves the identification of lorentzian components in the frequency spectrum. Time averaging was used to obtain accurate frequency spectra and data fitting was done by computer. Cross-correlation terms between weak lorentzians may be avoided and signal strength increased by employing the scattering of large particles dispersed in the solution as a local oscillator. Such a local oscillator source was naturally present in our RNase samples due to the aggregated protein. The more general usefulness of this effect was checked by measuring the diffusional scattering of dilute solutions of bovine serum albumen (BSA) to which was added very small concentrations of polystyrene latex spheres.

THEORETICAL CONSIDERATIONS

In this section we summarize the basic arguments that lead to the expressions used to analyze experimental data obtained in self-beat spectroscopy (1, 4, 5). The output current of the photomultiplier detector is proportional to the total photon flux impinging on the photo cathode, without consideration of the dark current; this is a good approximation with the high signal levels available from light scattered by macromolecular solutions. The flux per unit area is given for quasi-monochromatic light by the Poynting vector averaged over a period of the carrier frequency, in our case the frequency of the incident laser light. At the photomultiplier the electric field of the light scattered by diffusional fluctuations has the form (4)

$$\mathbf{E}_s(t) = \mathbf{E}(t)e^{i\omega_0 t}, \tag{1}$$

where ω_0 is the incident laser frequency and $\mathbf{E}(t)$ is the field amplitude which has a time dependence reflecting the random fluctuations in the concentrations, orientations, and shapes of the scattering macromolecules. Scattering due to fluctuations in dielectric constant of the solvent are negligible when compared to those from the macromolecules investigated in this experiment. $\mathbf{E}(t)$ may be taken as a real function and the photomultiplier (PM) current can be written as

$$J(t) = CS\mathbf{E}_s^*(t)\cdot\mathbf{E}_s(t) = CS\,|\,\mathbf{E}(t)|^2, \tag{2}$$

where S is the active area of the photo cathode and C is an instrumental constant.

The processes responsible for the time dependence of the $\mathbf{E}(t)$ are random and stationary in nature. Therefore the PM current will also be a stationary random function. We are interested in the power frequency spectrum of the $\mathbf{E}(t)$, which will determine that of $J(t)$. Such a power spectrum gives the power amplitudes of the harmonic components of $J(t)$.

The photocurrent power spectrum is given by (6)

$$I(\omega) = \int_{-\infty}^{\infty} e^{-i\omega t}\langle J(t)J^*(t+\tau)\rangle\, d\tau, \tag{3}$$

where the brackets $\langle\ \rangle$ indicate an ensemble average. For a stationary process this latter average is independent of t. Accordingly, from equation 2 we have

$$I(\omega) = C^2S^2 \int_{-\infty}^{\infty} e^{-i\omega t}\langle E_s(0)E_s^*(0)E_s(t)E_s^*(t)\rangle\, dt. \tag{4}$$

For a calculation of the scattered field the reader is referred to Peccora's paper (4). We only state the result here.

Let $\mathbf{K} = \mathbf{k}_s - \mathbf{k}_0$ be the transferred wave vector and c the velocity of light in the medium. To a good approximation

$$K = 2k_0 \sin(\theta/2) \tag{5}$$

where θ is the scattering angle within the medium. The frequency shift of the scattered light is small compared to ω_0, so

$$|k_0| = \frac{2\pi n}{\lambda_0} \simeq |k_s|, \tag{6}$$

where λ_0 = wavelength of incident light and n = index of refraction of medium.

The scattered field amplitude is given as a function of K (and therefore of the scattering angle) by equation 5 (4):

$$\mathbf{E}_s(\mathbf{K}, t) = \frac{\omega_0^2 E_i \sin(\mathbf{E}_i, \mathbf{k}_s)}{8\pi^2 c^2} \frac{\exp(ik_s R)}{R} \int_v d^3\mathbf{r} \exp[i\mathbf{K}\cdot\mathbf{r}]\epsilon_1(\mathbf{r}, t). \tag{7}$$

The integration in $d^3\mathbf{r}$ extends over the part of the sample volume where the incident field $\mathbf{E}_i \neq 0$. $\mathbf{E}_i$ is assumed to be uniform over this volume. R is the average distance of the point at which $\mathbf{E}_s$ is measured to the scattering volume and is a constant of the experimental setup. The scattered field has the form of a spherical wave, but with amplitude and frequency spectrum dependent on the scattering angle, through $\mathbf{K}$ and $\mathbf{k}_s$.

For a given scattering direction we can obtain the photocurrent power spectrum $I(K, \omega)$ by substituting equation 7 into equation 4. The spectrum $I(K, \omega)$ will consist of all possible heterodyne beats between the many Fourier components of the scattered field (7). Field components originating at different points in the scattering volume separated by a distance d will only give an effective beat signal over a photocathode of area $S \sim L^2$ if (8) $d < \lambda R/L$. For source separation larger than $\lambda R/L$ the phase difference between the two waves given by proper handling of the factor $\exp(ik_sR)$ will oscillate over the detector area; as the source separation d increases beyond the above limit the amplitude of the signal at the beat frequency does not increase. Thus, we divide the scattering volume into an ensemble of coherence volumes $\sigma < \lambda^3R^3/L^3$, and calculate the spectrum $I_\sigma(K, \omega)$ from each of these ele-

ments. The total heterodyne spectrum will equal

$$I(K, \omega) = (V/\sigma)I_\sigma(K, \omega), \tag{8}$$

where V is the total scattering volume. Combinations of fields scattered from different elements σ will only give a frequency independent noise contribution to $I(K, \omega)$ and a DC (constant) component. We can use Peccora's results for the spectrum of the field correlation function (4) to obtain $I_\sigma(k, \omega)$ under the assumption of gaussian nature for the random process, so that

$$\langle E(0)E(0)E(t)E(t)\rangle \propto [\langle E(0)E(t)\rangle]^2.$$

Let us indicate, by simple arguments, the form of the field correlation function for a two component system. This function is, by equation 7, proportional to the correlation function of the spatial Fourier component with wave vector **K** of the fluctuating part ϵ_1 of the dielectric constant. We shall assume ϵ_1 to be isotropic. If both types of particles were rigid noninteracting spheres, the correlation function of ϵ_1, as represented by its spatial Fourier spectrum will consist of two time-dependent terms corresponding to the translation diffusion correlation functions for each component:

$$\int_\sigma d^3r\langle\epsilon_1(r, t)\epsilon_1(0, 0)\rangle \exp i(\mathbf{K}\cdot\mathbf{r}) = N_1\Gamma_1(K)e^{-t(K^2D_1)} + N_2\Gamma_2(K)e^{-t(K^2D_2)}, \tag{9}$$

where N_i, D_i, $\Gamma_i(K)$ are, respectively, the number of particles in σ, the diffusion constants and the static scattering form factors for particles of species i. The PM current correlation function will be proportional to the square of equation 9:

$$I_\sigma(K, t) = \chi C^2S^2\{N_1^2\Gamma_1^2e^{-2tD_1K^2} + 2N_1N_2\Gamma_1\Gamma_2e^{-t(D_1+D_2)K^2} + N_2^2\Gamma_2^2e^{-2tD_2K^2}\}. \tag{10}$$

For rigid nonreacting particles the power spectrum of the total photomultiplier current will be:

$$I(\mathbf{k}, \nu) = G\left\{\frac{N_1^2\Gamma_1^2(2\Delta_1)}{\nu^2 + (2\Delta_1)^2} + \frac{2N_1N_2\Gamma_1\Gamma_2(\Delta_1 + \Delta_2)}{\nu^2 + (\Delta_1 + \Delta_2)} + \frac{N_2^2\Gamma_2^2(2\Delta_2)}{\nu^2 + (2\Delta_2)^2}\right\}, \tag{11}$$

where we have used frequencies instead of angular frequencies, to conform with the form of the experimental data.

$$\omega = 2\pi\nu, \qquad 2\pi\Delta_i = D_iK^2$$

and

$$2\pi G = (\nu/\sigma)\chi C^2S^2. \tag{12}$$

Thus, in general for such a two component system the experimentally measured spectrum will be fitted by a superposition of three different lorentzian components.

The following particular case will be of direct interest in connection with the present work. Γ_i increases extremely fast with increasing molecular size r (9) ($\Gamma_i \sim r^4$ for $r \ll \lambda_0$ and much faster as r approaches $\lambda_0/2$, λ_0 being the wavelength of the incident radiation). Thus, the following inequality may hold

$$N_1^2\Gamma_1^2 \gg N_2^2\Gamma_2^2, \tag{13}$$

even if $N_1 \ll N_2$, i.e., the larger particles are present in much lower concentration than the smaller ones. Then we may neglect the last term in equation 11; furthermore, since the diffusion constant of the larger particle is usually small compared to that of the smaller one, we will also have

$$\Delta_1 \ll \Delta_2$$

and thus the contribution to the spectrum of the first lorentzian in equation 11 will be concentrated in the lower frequency region.

If there is any chemical equilibrium involving the various components the N_1^2, N_1N_2, N_2^2 should be replaced by the appropriate number correlation functions which will have a time dependent part.

$$\langle N_i(0)N_j(t)\rangle = N_i(0)N_j(0) + \langle \delta N_i(0)\delta N_j(t)\rangle. \tag{14}$$

For a particle with internal motion, the Γ_i itself will contain a time dependent contribution:

$$\Gamma_i = \Gamma_{i,0}(K) + \Gamma_{i,1}(K, t). \tag{15}$$

The presence of these additional fluctuating contributions in equations 14 and 15 will entail additional lorentzian components in the spectrum. Their width will be larger than the corresponding diffusion width $2\pi\Delta_i = D_iK^2$ by some linear combination of reaction-rate constants and damping constants associated with modes of internal motion. Such spectral components can, in principle, be identified by the fact that the dependence of their widths deviates from the proportionality to K^2. The intensities of these components are expected to be much smaller than the intensity of those due to the time independent terms in equations 14 and 15 (the pure translatory diffusional spectrum), except perhaps where the total number of particles in the volume σ is so small that the fluctuations in this number become comparable to its average. Considerations of the absolute scattering intensities indicate that such a situation may indeed arise for particles with linear dimensions that are not negligible compared to λ_0.

EXPERIMENTAL

A block diagram of the time averaging frequency analyser apparatus is shown in Fig. 1. It is similar to that mentioned in reference (1) with the addition of time averaging (10).

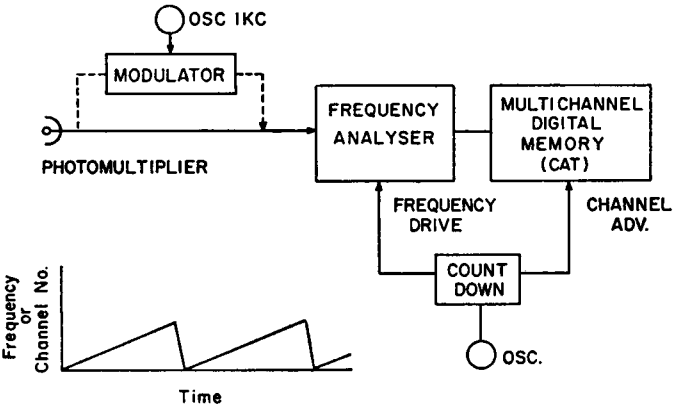

FIGURE 1 Block diagram of the time averaging frequency analyser arrangement.

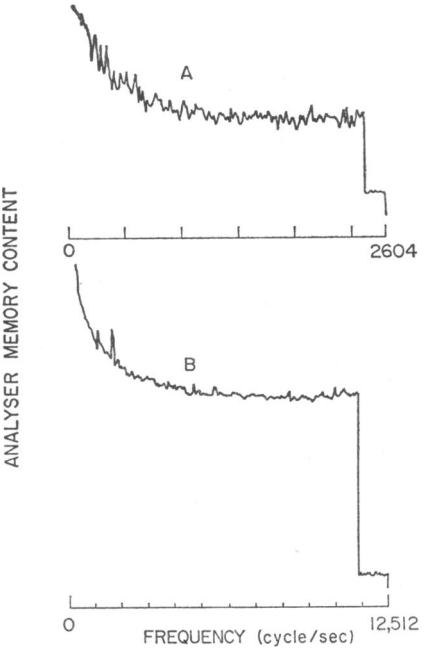

FIGURE 2 *A*—RNase 3%, T = 62.5°C, scattering angle 45°; *B*—RNase 3%, T = 24°C, scattering angle 45°. The short flat section at the end of each spectra is obtained with the General Radio analyser (General Radio Company) input shorted to obtain the location of the zero signal level in the analyser memory.

This procedure minimizes effects of low frequency instabilities of the PM and laser and allows almost indefinite accumulation periods resulting in high dynamic range. The light source was a 15 mw He-Ne laser (Spectraphysics model 124). The frequency analyser was a General Radio model 1800 A (General Radio Company, West Concord, Mass.). The frequency analyser was automatically scanned through the frequency range by a pulse controlled stepping motor, successive scans being stored in the memory of a Technical Measurements Corporation model CAT 1000 computer of average transients (Technical Measurements Corp., North Haven, Conn.). Memory contents of the CAT 1000 were trans-

ferred by paper tape to a time sharing computer where squaring, smoothing, and lorentzian curve fitting were performed.

The study of signals at frequencies below 10 Hz was hampered by the residual carrier unbalance and lack of response of the frequency analyser. For the study of this low frequency region the spectral range of the PM output was shifted to the 1 kHz region by modulation of the PM current with an oscillator (Fig. 1) (11). The spectrum of interest then appears in the form of side bands on the 1 kHz modulation, and may be more accurately resolved by the 3 Hz bandwidth of the frequency analyser.

The RNase A, purchased from Nutritional Biochemicals Corporation, Cleveland, Ohio, has been characterized as homogeneous protein by electrophoretic, chromatographic, and biochemical assays. Owing to the fact that the results obtained in the course of these experiments indicated that the enzyme solutions did have two components of differeng molecular size, we passed some of our solutions (in 0.5 M KCl) through a column packed with Sephadex G-75 (Pharmacia Fine Chemicals, Uppsala, Sweden) in accordance with procedures sug-

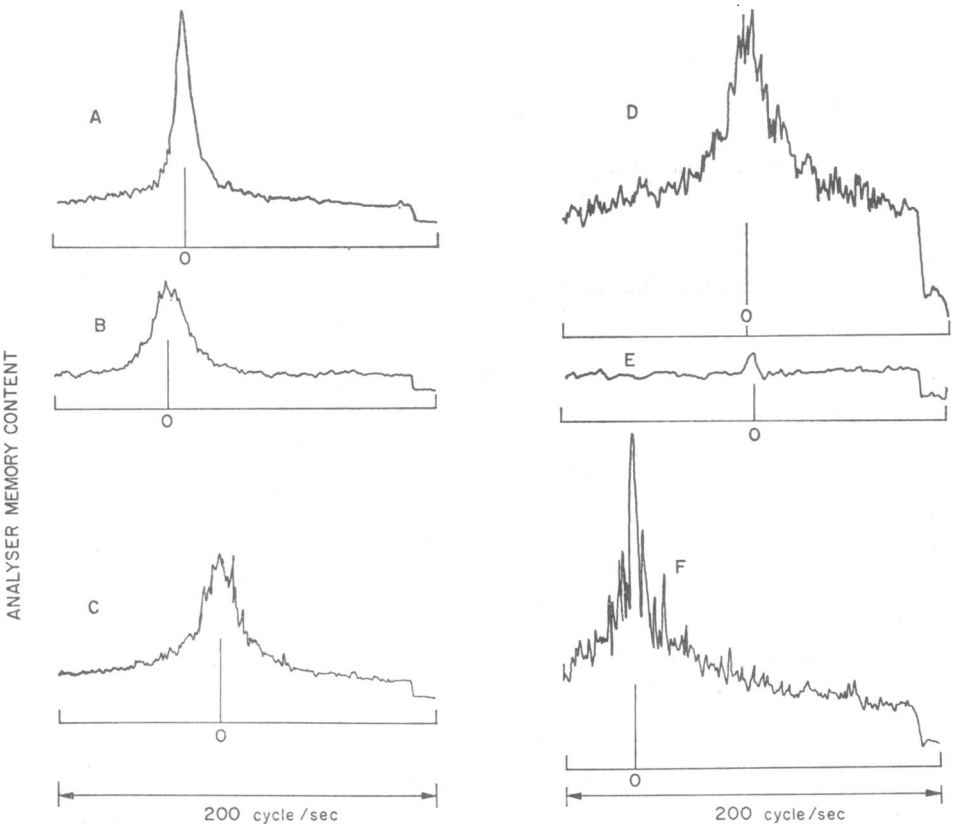

FIGURE 3 Low frequency data with second heterodyning; total scan 200 Hz. The initial points are not the same for all scans. At room temperature $A \rightarrow 7.5°$, $B \rightarrow 14.9°$, $C \rightarrow 22.1°$, and $D \rightarrow 45°$, scattering angles. $E \rightarrow$ same as D at room temperature but empty cell; E shows dark current, stray light, and residual carrier unbalance. $F \rightarrow T = 55°$, $45°$ scattering angle.

gested by Crestfield et al (12). The light scattering spectrum of the solution obtained at the elution volume corresponding to the RNase monomers was also studied and still showed that we had the two component system. The indication therefore was that the large particle component will appear after a reasonably short time (less than the time of elution through the column) in an equilibrium concentration sufficiently large to be detectable in our experiments. This point will be discussed later in some detail.

All samples were dissolved in 0.5 M KCl which had been previously cleaned of suspended material by vigorous shaking with CCl_4. The solutions were filtered through a fine fritted glass and various mesh size millipore filters before the measurements. Most measurements were carried out at pH $\simeq$ 8.1.

Fig. 2 shows typical readouts of the CAT 1000 memory content for RNase-0.5 M KCl solutions. Near the end of each trace the input to the frequency analyser was grounded to obtain true zero. Knowledge of the zero level is required when squaring (1) the data.

Fig. 3 shows typical data on RNase using the frequency upshift method. The center of the peak occurs at the modulating frequency of 1 kHz. Each spectrum covers a scan range of 200 Hz.

Fig. 4 shows data obtained on solutions of bovine serum albumen with and without a small addition of polystyrene latex spheres. These experiments were done to simulate the conditions encountered in the RNase samples of a two-component system with one much larger than the other. Sizes and concentrations of the two components satisfy the conditions for the validity of expression (13). The higher frequency lorentzian component in the mixed samples will yield the diffusion spectrum of the BSA molecules but with a line width of D_2K^2 rather than $2D_2K^2$ and the amplitude increase over that of a single lorentzian sample

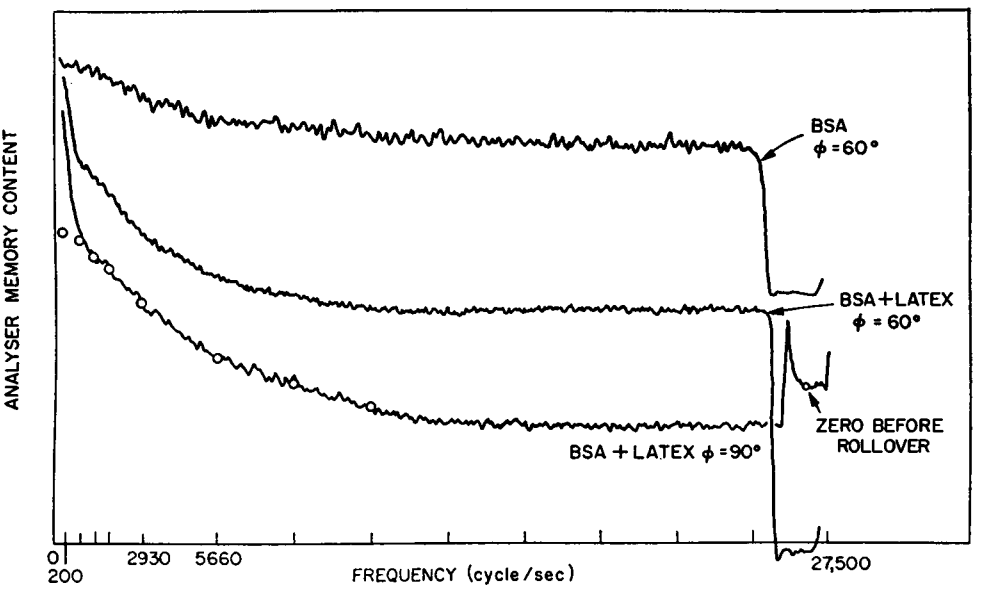

FIGURE 4 ϕ's are external angles, i.e., angle between the laser beam and the scattered light outside the sample cell. ϕ = 60° corresponds to a scattering angle inside the sample cell of 67.9°. Top: Solution of bovine serum albumen (BSA) at 3% weight. Middle: BSA at 1% + latex spheres. Bottom: BSA at 1% + latex spheres. (For this trace this difference between the spectrum and the zero level includes one complete fill of the analyser memory.)

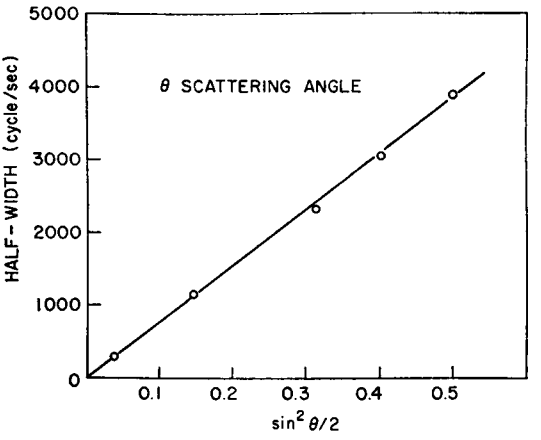

FIGURE 5 Diffusion half-width Δ_2 of the weaker lorentzian in BSA and latex sphere solutions.

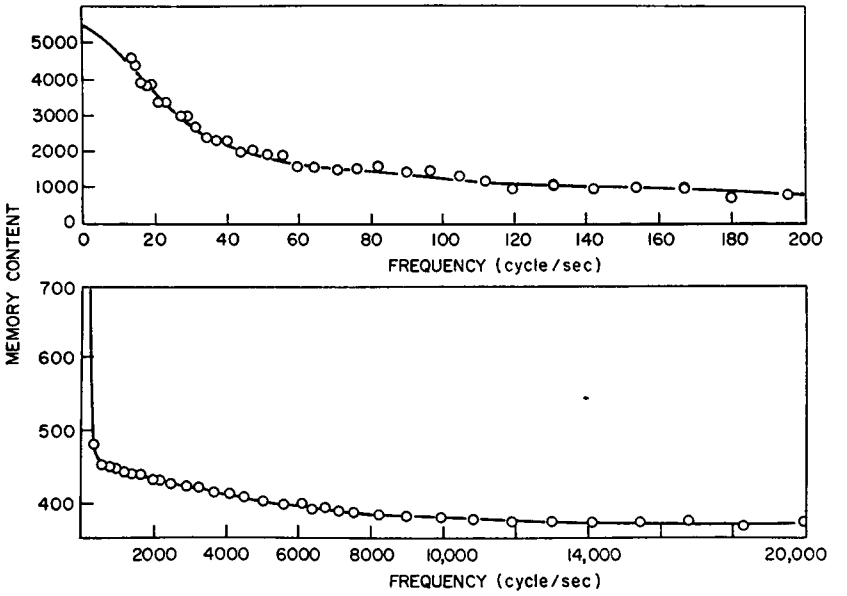

FIGURE 6 Circles—squared and smoothed data; RNase 3%, scattering angle of 67.9°. Solid line—calculated best fit, $2\Delta_1 = 22$ Hz, $\Delta_2 = 4660$ Hz.

will be $(N_1\Gamma_1/N_2\Gamma_2)$. These effects are shown in the two upper traces of Fig. 4. BSA concentration was 1% in the mixed solutions, whereas it was 3% in the pure sample. The concentration of 0.109 μ polystyrene latex spheres was less than 0.003%. Computer fitting of the squared signals yielded values for Δ_2 and these values are plotted as a function of $\sin^2(\theta/2)$ in Fig. 5. For $(\omega/2\pi) > 200$ Hz the inequality $(\Delta_1/2\pi) \ll \omega$ allowed us to represent the narrow lorentzian by the expression (constant/ω^2). The quality of this type of fit is shown by the calculated points for the 90° data on Fig. 4. The BSA diffusional constant obtained from the Δ_2 plot of Fig. 5 is $D = 6.75 \pm 0.10 \times 10^{-7}$ cgs units in good agreement with Benedek's value of 6.7×10^{-7} (3).

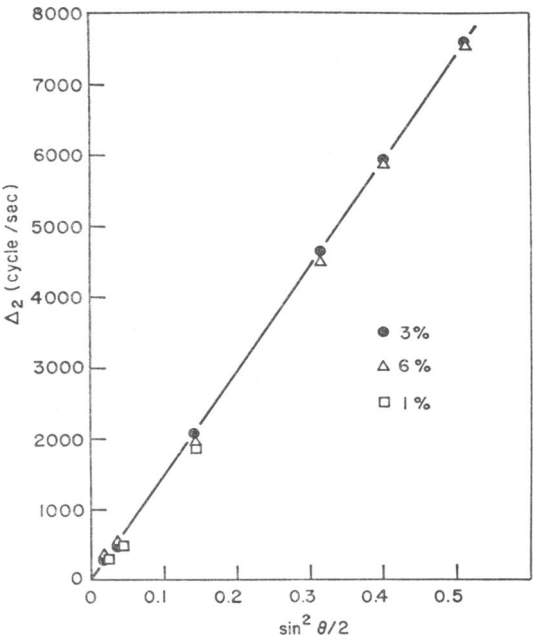

FIGURE 7 Diffusional width of RNase molecules; ϕ = scattering angle.

Fig. 6 shows, for a typical case (3% RNase solution, scattering angle of 67.9°, room temperature) the computer output points after squaring and smoothing. None of the RNase spectra could be fitted by a single lorentzian. The continuous trace shows a minimum mean-square error fit with two lorentzians for which $2\Delta_1 = 22$ Hz, $\Delta_2 = 4660$ Hz.

It was clear from these data that we were dealing with a two-component spectrum, one with half-width below 50 Hz, and the other which roughly corresponded to the expected diffusion spectrum for small protein molecules such as RNase. For each set of conditions expanded data were taken between the lowest possible frequency (about 10 Hz at 3 Hz bandwidth of the frequency analyzer) and about 200 Hz. This region could be fitted quite well with a single lorentzian. Next, measurements were made with high gain to a sufficiently high frequency to obtain most of the tail of the lorentzians. The resulting data were fitted with two lorentzians, with half-widths $2\Delta_1$ and Δ_2. The amplitude of both and the half-width Δ_2 were taken as parameters. This second fitting was rather insensitive to Δ_1 since through most of the frequency domain the corresponding lorentzian had the general form (constant/ω^2) with ($\omega \gg \Delta_1$). We should add that in all cases a constant had to be added to equation 11 to fit the frequency independent shot-noise contribution present in all data.

The low frequency limitation in these measurements was the frequency analyzer. The shape of the low frequency component therefore was rechecked by measuring the spectra after frequency upshift to 1000 Hz. The low frequency data, at least up to 55°C, indicated that a reasonable fit could be obtained with a single lorentzian and that the results of the measurements without the 1000 Hz upshift were essentially correct. Figs. 7 and 8 show plots of $\Delta_2 - \Delta_1 \simeq \Delta_2$ and $2\Delta_1$ as a function of $\sin^2 \theta/2$ at room temperature for three concentrations. For Δ_2 (Fig. 7) it is clear that we are dealing with translational diffusion since the data is well fitted by a straight line, with Δ_2 proportional to $\sin^2 \theta/2$ (3).

The experimental uncertainty for the widths on Fig. 8 is in the order of ± 2.5 Hz. A straight line fit to the complete set of points yields a nonzero intercept at zero frequency, indicating a

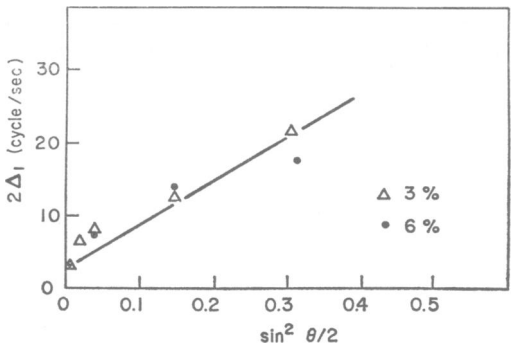

FIGURE 8 Half-width $2\Delta_1$ of the low frequency component in RNase; ϕ = scattering angle.

finite broadening at θ or $K = 0$. This effect would be even more pronounced if the lowest angle datum were to be disregarded. The neglect of this point has some justification due to the difficulty at this small angle of completely preventing the laser light originating from scatter at the cell walls from hitting the detector. In any case the presence of a nontranslational factor in the spectrum from these large particles seems to be indicated by the data.

We should note at this point that whereas the widths were essentially independent of concentration between 1 and 6% (g/100 cc), the ratio of intensities of the low to the high frequency component increases by over an order of magnitude as a function of concentration in this range, indicating that the scattering centers responsible for it may result from aggregation of RNase molecules. The fact that a single lorentzian yields a good fit does not guarantee that the low frequency spectrum is due to a truly monodisperse system. Since the intensity decreases rapidly with decreasing particle size, the observed low frequency scattering probably is only a measure of scattering by the largest particles. The diffusion coefficient however is a slow function of particle size, which may account for observation of a single lorentzian even with some polydispersity for these large particles. The concentration of large particles is extremely small; equivalent intensity is obtained from a 0.1 μ latex sphere solution of about 0.001%.

A small concentration (a few per cent or less) of low polymers (dimers, trimers) may also easily escape observation since, for these, the enhancement in light scattering cross-section over that for the monomers is not sufficient to overcome the concentration effect.

The spectrum was found to be essentially independent of pH between 8.2 and 2.

DISCUSSION OF THE DATA ON RNASE

Using the methods discussed in the previous section, we have analyzed the data for the diffusion constant of the individual RNase molecules. We should here stress the fact that no matter what the detailed interpretation of the low frequency component, we obtain through equation 11 correct values for the diffusion width. The low frequency component of the scattered light may be considered simply as a heterodyning signal. As the data in Fig. 7 show, there is no measurable concentration dependence of the diffusion constant between 1 and 6% RNase. Thus we can assume the diffusion constant obtained by these experiments to apply at infinite dilution. At 24°C we obtain $D = 12.6 \times 10^{-7} \pm 0.10$ cgs units, which is in reasonable agreement with the previously published value of 11.9×10^{-7} at 20°C (13).

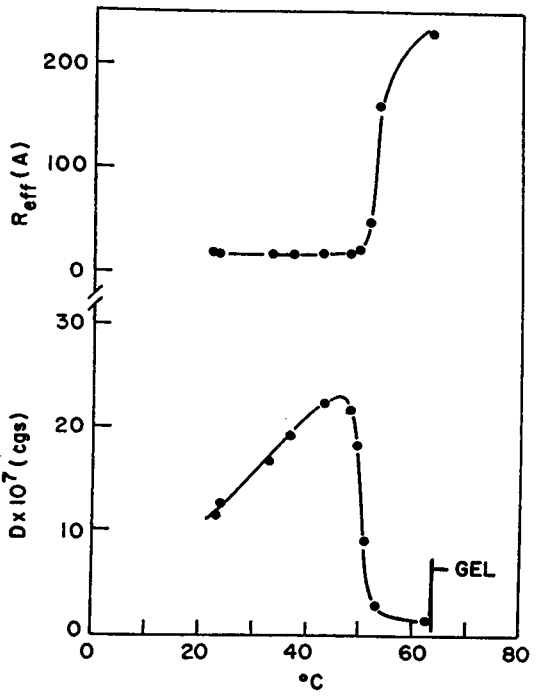

FIGURE 9 Temperature dependence of diffusion constant and molecular size of RNase.

In Fig. 9 we show the temperature dependence of this diffusion constant. Up to about 62°C the value of D is reversible, i.e. if the sample is returned to 24°, and the new data is fitted, the width of the high frequency component yields the same value of D. The same is not necessarily true of the intensity and the width of the low frequency component. Above 63° the whole sample gels very rapidly and irreversibly.

Using the Stokes relation (14) between the diffusion constant and the friction coefficient, and assuming an effective spherical shape for the molecules, one can deduce an effective radius (R_{eff}) for the RNase;

$$R_{eff} = (kT)/(6\pi\eta D),$$

where η is the solvent viscosity.

In the denatured states the molecules are probably far from spherical, thus R_{eff} is only an average quantity. Nevertheless, it serves to characterize molecular size just as do results of intrinsic viscosity (14–16). The onset of denaturation is clearly indicated by the sharp rise in R_{eff}, starting at about 50°C where the molecule seems to have expanded about an order of magnitude before irreversible processes become dominant. This increase in R_{eff} (from 20 to about 250 A) may indicate the degree of "uncoiling" due mainly to the disruption of internal bonds.

In order to check this latter effect we also performed measurements on samples

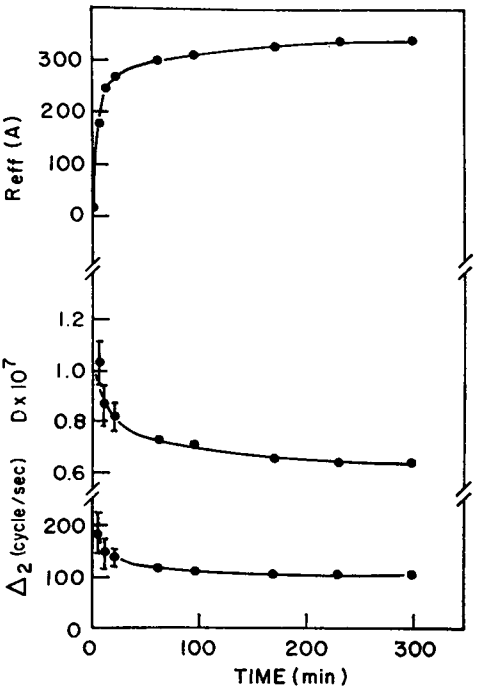

FIGURE 10 Diffusion constant and effective size of 1% RNase in 10 M urea as a function of time elapsed after mixing.

denatured by reaction with a high concentration of urea (17). We used 10 M urea and the smallest possible RNase concentration (about 1%) to insure that we reach stable conditions rapidly. A plot of D as a function of time elapsed after sample preparation is shown on Fig. 10. Corresponding values of R_{eff} are also shown in Fig. 10; these were computed under the assumption that there was no significant change in the viscosity of the solvent. The large error bars on the initial few points are indicative of unstable conditions. The same order of change in R_{eff} is observed here as in the thermal denaturation, indicating that the extent of the uncoiling of the protein molecule is similar in both cases. The final product of urea denaturation is not expected to be the same as in thermal denaturation (18, 19). The amount of solvated water may consequently be also quite different, all of this affecting the effective molecular size.

Turning to the room temperature low frequency component, we have already shown, in Fig. 3, typical data obtained by the frequency upshift technique. At the lower temperatures we obtain an approximate single lorentzian fit. This, however, cannot be taken as proof that we have a monodisperse system, since in the effective size range we are dealing with the scattered intensity decreases so rapidly with decreasing particle size (9) (at least as R^4) that the spectrum observed could easily be dominated by the largest particles. Since the *line width*, whether due to translational diffusion or some other interaction, is expected to be a relatively slow func-

tion of size, a single lorentzian from large particles may be observed even with appreciable polydispersity.

From the computer fits we can obtain the peak intensity of the low frequency component relative to that of the high frequency component. The spectrum with two components will have the general form given by the first two terms in equation 11, with Δ_1 and Δ_2 appropriate functions of K. For individual molecules which are small compared to wavelength, Γ_2, the amplitude of the small molecule component, is quite insensitive to K (9) (this should be a good approximation for 20 A particles). Thus, from the knowledge of $\Delta_1(K)$ and $\Delta_2(K)$ and the ratio of intensities for the first two components, we obtain $(N_1\Gamma_1[K]/N_2\Gamma_2)$ which should be, to a good approximation, proportional to the angular factor in the intensity of light scattered by the large molecular component. Such ratios also become comparable for samples of different concentrations, since we know $N_2\Gamma_2$ will be linear in RNase concentration. Fig. 11 shows this ratio vs. angle for two concentrations. The dependence on

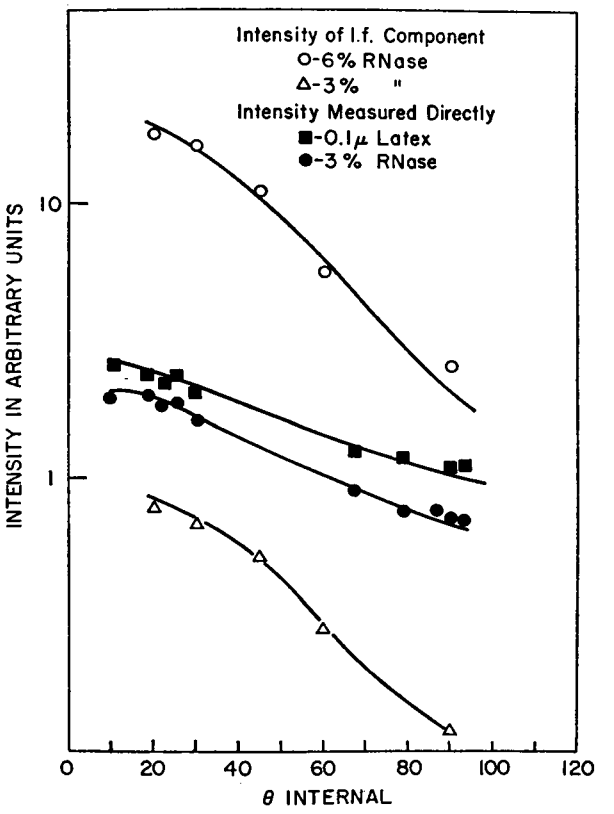

FIGURE 11 Top and bottom curves: $(N_1\Gamma_1/N_2\Gamma_2)$ of RNase at room temperature as a function of the scattering angle θ. Middle curves: total intensities corrected for refraction and apparent source length.

angle, and therefore on K, is the same for both concentrations. On the other hand for fixed angle, $N_1\Gamma_1$ increases with concentration much faster than linearly, indicating that scatterers responsible for the low frequency component result from association of smaller molecules. The table below shows this explicitly.

Concentration % RNase	$N_1\Gamma_1/N_2\Gamma_2$ ($\theta = 45°$)
1	0.25
3	0.5
6	11.0

Also in Fig. 11 we show angular dependence of total scattered intensity for the 3% RNase solution and for 0.1 μ latex spheres of about 0.001% concentration. The total intensities are comparable for both cases and the angular dependences are also similar. Information obtained from this comparison is only qualitative in nature. Nevertheless, it gives an indication that the particle size of the aggregates in the RNase is in the order of thousands of A, and that their concentration is in the order of one part in 10^5. The angular dependence of the ratio $N_1\Gamma_1/N_2\Gamma_2$ drops off at the larger angles faster than the total intensity indicating a somewhat larger diameter. This is not unexpected since the total scattering intensity includes the contribution of the RNase monomers which is essentially independent of scattering angle. Using, as an arbitrary measure of particle radius,

$$\bar{R} = 2\pi/\bar{K},$$

where $\bar{K}$ is the value of the transferred momentum at the angle $\bar{\theta}$ where the ratio $N_1\Gamma_1/N_2\Gamma_2$ drops to 10% of its value at $\theta = 0$, we obtain $\bar{R} \simeq 3000$ A.

Assuming that the entire width Δ_1 is due to translational diffusion (a good approximation at larger angles), we can obtain temperature-dependent effective diffusion constants and R_{eff}'s which are shown in Fig. 12. Thus we see that the estimate of $\bar{R}$ from the angular dependence of the intensity ratio of Fig. 11 is not too far from the values obtained using the Stokes equation.

At the higher temperatures (above 55°) we see in Fig. 3 *F* the appearance of an even narrower component in the spectrum. This is possibly due to the formation of aggregates larger than the 3000 A particles mentioned above.

More information on the nature of these large particles was obtained in the following experiment. The frequency spectrum of a fresh sample was measured. The sample was heated to 65° for a time sufficiently short that no visible gel formation took place (about 5 min). The line width of the two components did not change, $2\Delta_1$ and Δ_2 remaining at 22 and 4660 Hz. However, the room temperature value of $N_1\Gamma_1/N_2\Gamma_2$, at $\theta = 45°$, went from 0.5 to 3.66. This indicates a marked increase of the

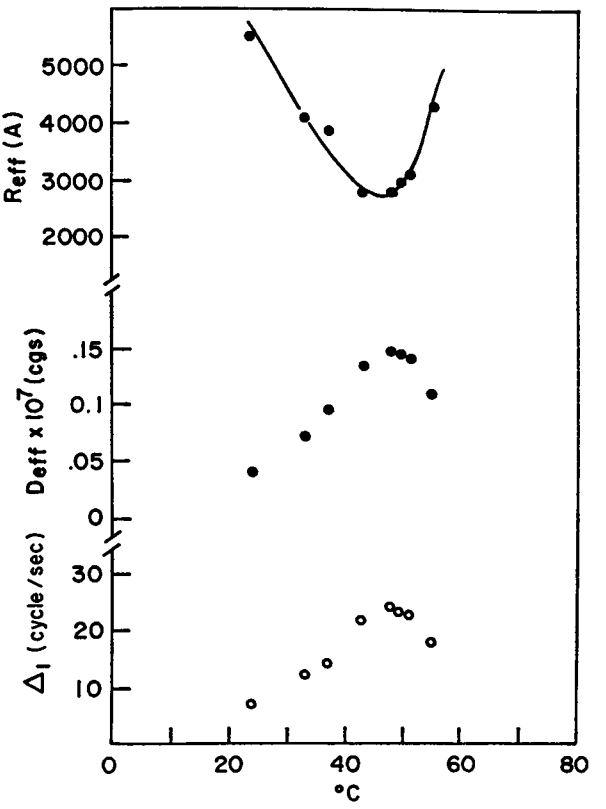

FIGURE 12 Temperature dependence of apparent diffusion constant and effective size obtained from the width $2\Delta_1$ of the low frequency component of the RNase spectrum at $\theta = 45°$.

large particle concentration when the temperature is elevated to the region of irreversible denaturation.

To recapitulate, we find strong indication that in the case of RNase, even in relatively fresh samples, at room temperature there is a measurable concentration of denatured material which tends to associate in rather large particles, some as large as 3000 A. This value of 3000 A is really an upper limit due to size effects in scattering efficiency. The peculiar temperature dependence of R_{eff} in Fig. 12 could be due to a number of effects. First, it appears that the line width has a nontranslational contribution (Fig. 8). Secondly, the initial decrease of R_{eff} (Fig. 12) with T may be due to decrease in the quantity of solvated water. Thirdly, these are rather large and probably loosely bound aggregates with large amounts of bound water; certainly the Stokes relation will be far from accurate in this case. Detailed interpretation of the low frequency spectral component requires some model applicable to such large, presumably nonrigid, molecules where translational, rotational, and internal motion are not readily separable.

CONCLUDING REMARKS

Using quasi-elastic light scattering spectra, we have investigated diffusional fluctuations of RNase. These measurements were performed at different temperatures and also in the presence of urea as a denaturing agent.

The diffusion coefficient for individual protein molecules, together with the corresponding calculated effective molecular radius R_{eff}, were determined throughout the region of reversible denaturation. Between room temperature and the point of irreversible denaturation at 63.5°C, R_{eff} increased from 20 to 250 A. This is comparable to the plateau in R_{eff} of 300 A reached after about 200 min following chemical denaturation in 10 M urea. These results indicate that even though the detailed mechanism involved in the two denaturation reactions may be different, the degree of configurational expansion is about the same.

If the change in R_{eff} upon denaturation obtained in this work is taken as an indication of the corresponding change in hydrodynamical volume, the present results predict a much larger change in intrinsic viscosity upon denaturation than that of a factor of 3 observed by Harrington and Schellman (20). Both properties depend on an average hydrodynamic molecular shape; the apparent discrepancy indicates that the many possible molecular configurations are weighted differently in the two averages. The above authors also find similar discrepancies when attempting to extract effective axial ratios from different properties of denatured RNase molecules. It is of interest to note that the change in R_{eff} upon urea denaturation in the present work is also much larger than that observed for lysozyme by the same technique (21).

The measurements indicated the presence of large particles even in the freshly prepared and chromatographically purified RNase solutions. From the diffusion constants deduced for this large component, we obtained effective apparent sizes from 1000–5000 A (depending on temperature). Angular dependence obtained for the intensity of the spectral component due to these large particles confirmed these estimates for their size. Concentration and temperature dependence of the large particle scattering exclude the possibility that these particles are impurities and indicate that they are the result of aggregations of RNase molecules. The spectrum of fluctuations due to these aggregates appears to contain a nontranslational contribution.

It may be that the increase in size in the reversible stage of the denaturation process represents a molecular conformation change essential to subsequent aggregation. The size of the aggregate may, upon reaching an upper limit in the range of 5000 A, determine gelation. We are currently examining other macromolecular systems more specifically designed to yield information concerning the dynamics of protein aggregation processes.

We wish to thank Mr. R. Freehling for carrying out the initial experiments and Mr. R. Kilponen for expert technical assistance, and Drs. G. B. Benedek and J. L. Oncley for enlightening discussions.

Received for publication 26 June 1969.

REFERENCES

1. FORD, N. C., and G. B. BENEDEK. 1965. *Phys. Rev. Lett.* **15**:649.
2. LASTOVKA, J. B., and G. B. BENEDEK. 1966. *Phys. Rev. Lett.* **17**:1039.
3. DUBIN, S. B., J. H. LUNACEK, and G. B. BENEDEK. 1967. *Proc. Nat. Acad. Sci. U.S.A.* **57**:1164.
4. PECCORA, R. 1964. *J. Chem. Phys.* **40**:1604.
5. PECCORA, R. 1968. *J. Chem. Phys.* **48**:4126.
6. WANG, M. C., and G. E. UHLENBECK. 1945. *Rev. Mod. Phys.* **17**:323.
7. FORRESTER, A. T. 1961. *J. Opt. Soc. Amer.* **51**:253.
8. FORRESTER, A. T. 1956. *Amer. J. Phys.* **24**:192.
9. VAND DE HULST, H. C. 1957. Light Scattering by Small Particles. John Wiley and Sons, Inc., New York.
10. ERNST, R. R. 1965. *Rev. Sci. Instrum.* **36**:1689.
11. ARECCHI, I. T., M. GIGLIO, and U. TARTARI. 1967. *Phys. Rev.* **163**:186.
12. CRESTFIELD, A. M., W. H. STEIN, and S. MOORE. 1962. *Arch. Biochem. Biophys. Suppl.* **1**:217.
13. ROTHEN, A. 1940. *J. Gen. Physiol.* **24**:203.
14. TANFORD, C. 1961. Physical Chemistry of Macromolecules. John Wiley and Sons, Inc., New York. 349.
15. SCHACHMAN, H. K. 1963. *Cold Spring Harbor Symp. Quant. Biol.* **28**:409.
16. TANFORD, C. 1961. Physical Chemistry of Macromolecules. John Wiley and Sons, Inc., New York. 395, 626.
17. TANFORD, C. 1961. Physical Chemistry of Macromolecules. John Wiley and Sons, Inc., New York. 627–639.
18. TANFORD, C. 1964. *J. Amer. Chem. Soc.* **86**:2050.
19. BRANDTS, J. F., and L. HUNT. 1967. *J. Amer. Chem. Soc.* **89**:4826.
20. HARRINGTON, W. F., and J. A. SCHELLMAN. 1956. *C. R. Trav. Lab. Carlsberg.* **30**:21.
21. DUBIN, S. B., G. FEHER, and G. B. Benedek. 1969. Abstracts of the Biophysical Society 13th Annual Meeting. Los Angeles, California. 213.